Journal of Systems Engineering and Electronics
Vol. 33, No. 1, February 2022, pp.134 – 143

An anti-main-lobe jamming algorithm for airborne early warning radar based on APC-SVRGD joint optimization

PENG Fang[1], WU Jun[2,*], WANG Shuai[1], LI Zhijun[1], and XIANG Jianjun[1]

1. Aviation Engineering School, Air Force Engineering University, Xi'an 710038, China;
2. Air Traffic Control and Navigation School, Air Force Engineering University, Xi'an 710051, China

Abstract: Main lobe jamming seriously affects the detection performance of airborne early warning radar. The joint processing of polarization-space has become an effective way to suppress the main lobe jamming. To avoid the main beam distortion and wave crest migration caused by the main lobe jamming in adaptive beamforming, a joint optimization algorithm based on adaptive polarization canceller (APC) and stochastic variance reduction gradient descent (SVRGD) is proposed. First, the polarization plane array structure and receiving signal model based on primary and auxiliary array cancellation are established, and an APC iterative algorithm model is constructed to calculate the optimal weight vector of the auxiliary channel. Second, based on the stochastic gradient descent principle, the variance reduction method is introduced to modify the gradient through internal and external iteration to reduce the variance of the stochastic gradient estimation, the airspace optimal weight vector is calculated and the equivalent weight vector is introduced to measure the beamforming effect. Third, by setting up a planar polarization array simulation scene, the performance of the algorithm against the interference of the main lobe and the side lobe is analyzed, and the effectiveness of the algorithm is verified under the condition of short snapshot number and certain signal to interference plus noise ratio.

Keywords: airborne early warning radar, adaptive beamforming, main-lobe interference suppression, adaptive polarization canceller (APC), stochastic variance reduction gradient descent (SVRGD).

DOI: 10.23919/JSEE.2022.000014

1. Introduction

As the core sensor of the early warning aircraft, airborne early warning radars coordinately perform diversified combat tasks such as air alert, control guidance, combat command and air battlefield management. Air battlefield electronic countermeasures are becoming increasingly fierce. Aiming at side-lobe interference, radars are often suppressed effectively by ultra-low side-lobe antennas, beam width control, antenna coverage and scanning control, side-lobe blanking and side-lobe cancellation, and adaptive zeroing [1−5]. However, when they are subject to long-range support main lobe interference from electronic warfare aircraft, team-type main lobe interference, and airborne self-defense electronic interference, conventional adaptive beamforming algorithms form in the main lobe of the radar beam, leading to distortion of the main lobe, peak deviation, and increased side lobe level [6], which in turn reduces the output signal-to-interference and noise ratio, and the probability of false alarms sharply increases. At the same time, the peak deviation also affects angle measurement accuracy. Thus the performance of the algorithm is severely degraded and even fails. Therefore, main lobe jamming has become a preferred choice for the jamming style of electronic warfare equipment. The existing countermeasures are still limited, and effective countermeasures have not yet been formed, which severely restricts the combat performance of the radar. How to effectively suppress the main lobe interference has become an urgent task and a common problem in modern radar electronic countermeasures.

The polarization domain is another scope of radar signals in addition to the space-time-frequency energy domain. It has shown positive effects in suppressing main lobe interference, identifying active false targets, and countering angle decoy interference. The essence of polarization anti-main lobe interference is to use the difference between the interference and the target in the polarization domain when the target and the interference are not easy to be distinguished in the direction of the incoming wave, and to reduce or eliminate the influence of the interference on the radar detection. However, with the continuous upgrading of electronic countermeasures, the difference between the target and the interference is getting more and more subtle, and the ability to suppress the

Manuscript received November 05, 2020.
*Corresponding author.
This work was supported by the Aviation Science Foundation of China (20175596020).

main lobe interference only by polarization filtering is limited. Therefore, the polarization anti-main lobe interference method is shifted to multi-domain (polarization-space, polarization-space-time) joint processing [7−9]. In terms of polarization domain processing, Chen [10] proposed using interference sampling data to estimate the cancellation weight coefficients between the two polarization channels based on the minimum interference output power criterion. For adaptive interference polarization cancellation, Yang et al. [11] and Ren et al. [12] proposed using the main polarization and cross polarization receiving channels of fully-polarized auxiliary antennas, or using adaptive orthogonal virtual polarization technology to suppress interference and obtain better results. This method has a good interference rejection ratio. In spatial processing, intelligent optimization algorithms based on particle swarm optimization [13], neural network [14,15], and stochastic gradient descent (SGD) are applied to adaptive beamforming [16−18]. The algorithm convergence, beamforming performance and robustness show unique advantages.

The adaptive polarization canceller (APC) algorithm has matured day by day, and the main/auxiliary channel structure in the algorithm model is simple [19−21]. Currently airborne early warning radars mainly use active area array antennas. There are few literature reports on how to apply the polarization cancellation algorithm to the polarization array [22−25]. For the configuration of primary/secondary array structure, an intelligent optimization algorithm is used to improve the beam performance degradation caused by main lobe interference in polarization domain spatial joint processing [26−28]. Therefore, this article focuses on main beam distortion, peak shift, and sidelobe level increase caused by mainlobe interference in adaptive beamforming [29,30]. It proposes a polarized array adaptive beamforming based on the APC stochastic variance reduction gradient descent (APC-SVRGD) joint optimization method. First, establish the polarization area array structure and the received signal model based on the main/auxiliary array cancellation, derive the APC iterative algorithm flow, obtain the calculation method of the equivalent polarization weight vector, and eliminate the main lobe interference through polarization filtering. Second, in the spatial beamforming stage, the minimum mean square error criterion is adopted, the variance reduction method is introduced based on the principle of SGD. The gradient correction is performed through inner and outer loop iterations to reduce the variance of stochastic gradient estimation and improve the gradient estimation approximation. The purpose is to calculate the optimal weight vector in the airspace, and to weight all the array elements to obtain the array output. Through the combined processing of the polarization domain and the space domain, the effective suppression of the main lobe interference and the adaptive zeroing of the side lobe interference are realized. The SVRGD method can effectively improve the anti-jamming performance of beamforming. It is also suitable for situations where the objective function is non-differentiable and non-stationary.

2. Polarization area array APC algorithm based on steepest gradient descent

2.1 Polarized array antenna pattern

The polarization array can actually be regarded as the expansion of the polarization linear array in the two-dimensional space, as shown in Fig. 1. Each element is composed of two orthogonal electric dipoles. Assume that the electromagnetic wave is a fully polarized wave. It is represented by a polarized phase (γ,η) descriptor, where $\gamma\in[0,\pi/2]$, $\eta\in[0,2\pi]$. Place the polarization array vertically in the XOZ plane. The number of array elements is $M\times N$. The array element spacing in the vertical direction and the vertical directions are d_x and d_z respectively. Each array element is the same array element with precise position, consistent polarization characteristics, no coupling between the array elements, and the same array element channel amplitude. Assume that the internal noise of each array element channel is zero mean, the variance is a constant Gaussian white noise, the noise of each array element is independent, and the signal and noise are independent of each other.

Let the number of signal sources be K, and θ_i,φ_i represent the elevation angle and azimuth angle of the source respectively, $\Theta_i=(\theta_i,\varphi_i)(i=1,2,\cdots,K)$, as shown in Fig. 2. Among them, $0\leqslant\theta_i<90^\circ$, $0\leqslant\varphi_i<360^\circ$.

According to the analysis of the uniform linear array, the direction matrices on the X-axis and Z-axis are

$$\boldsymbol{A}_x=\begin{bmatrix}1 & 1 & \cdots & 1\\ \mathrm{e}^{-\mathrm{j}\frac{2\pi d_x\cos\varphi_1\sin\theta_1}{\lambda}} & \mathrm{e}^{-\mathrm{j}\frac{2\pi d_x\cos\varphi_2\sin\theta_2}{\lambda}} & \cdots & \mathrm{e}^{-\mathrm{j}\frac{2\pi d_x\cos\varphi_K\sin\theta_K}{\lambda}}\\ \vdots & \vdots & \ddots & \vdots\\ \mathrm{e}^{-\mathrm{j}\frac{2\pi d_x(N-1)\cos\varphi_1\sin\theta_1}{\lambda}} & \mathrm{e}^{-\mathrm{j}\frac{2\pi d_x(N-1)\cos\varphi_2\sin\theta_2}{\lambda}} & \cdots & \mathrm{e}^{-\mathrm{j}\frac{2\pi d_x(N-1)\cos\varphi_K\sin\theta_K}{\lambda}}\end{bmatrix},\tag{1}$$

$$\boldsymbol{A}_z=\begin{bmatrix}1 & 1 & \cdots & 1\\ \mathrm{e}^{-\mathrm{j}\frac{2\pi d_z\cos\theta_1}{\lambda}} & \mathrm{e}^{-\mathrm{j}\frac{2\pi d_z\cos\theta_2}{\lambda}} & \cdots & \mathrm{e}^{-\mathrm{j}\frac{2\pi d_z\cos\theta_K}{\lambda}}\\ \vdots & \vdots & \ddots & \vdots\\ \mathrm{e}^{-\mathrm{j}\frac{2\pi d_z(M-1)\cos\theta_1}{\lambda}} & \mathrm{e}^{-\mathrm{j}\frac{2\pi d_z(M-1)\cos\theta_2}{\lambda}} & \cdots & \mathrm{e}^{-\mathrm{j}\frac{2\pi d_z(M-1)\cos\theta_K}{\lambda}}\end{bmatrix}.\tag{2}$$

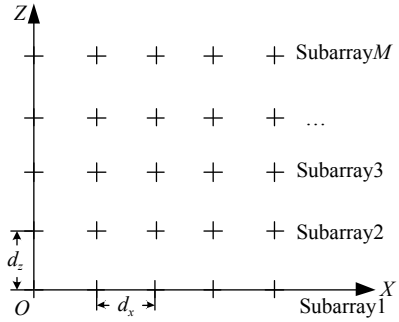

Fig. 1 Polarized area array structure

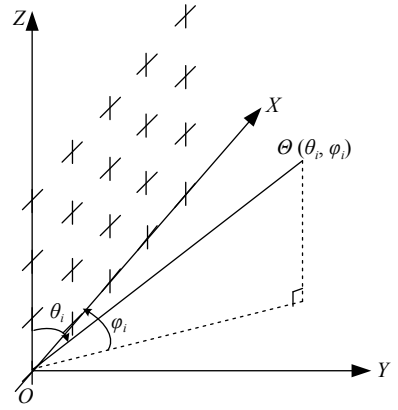

Fig. 2 Spatial geometric relationship of polarization array

The direction matrix of Subarray1 is $\boldsymbol{A}_x$, the phase difference of each element in Subarray2 with respect to the reference element is equal to the phase difference of the element in Subarray1 plus $-\mathrm{j}2\pi d_z \cos\theta_i/\lambda$, where λ is the wavelength of the incoming signal. Thus the direction matrix of the m subarray is $\boldsymbol{A}_m = \boldsymbol{A}_x \boldsymbol{D}_m(\boldsymbol{A}_z)(m = 1,2,\cdots,M)$, $\boldsymbol{D}_m(\boldsymbol{A}_z)$ is a diagonal matrix constructed by the Mth row of $\boldsymbol{A}_z$.

$$\begin{cases} \text{Subarrayl}, & \boldsymbol{A}_1 = \boldsymbol{A}_x \boldsymbol{D}_1(\boldsymbol{A}_z) \\ \text{Subarray2}, & \boldsymbol{A}_2 = \boldsymbol{A}_x \boldsymbol{D}_2(\boldsymbol{A}_z) \\ & \vdots \\ \text{Subarray}M, & \boldsymbol{A}_M = \boldsymbol{A}_x \boldsymbol{D}_M(\boldsymbol{A}_z) \end{cases} \tag{3}$$

The spatial direction matrix of the area array is

$$\boldsymbol{A}(\Theta) = [\boldsymbol{A}_1; \boldsymbol{A}_2; \cdots; \boldsymbol{A}_M] = [\boldsymbol{a}(\Theta_1), \boldsymbol{a}(\Theta_2), \cdots, \boldsymbol{a}(\Theta_K)]. \tag{4}$$

Assume that each element emits a transverse electric and magnetic (TEM) electromagnetic wave signal along the $\hat{r}$ direction, the complex baseband signal is $s(t)$, the carrier frequency is f, its spatial pointing angle is (θ, φ), and the unit vector $(\hat{\varphi}, \hat{\theta}, -\hat{r})$ form the right-hand coordinate system. The TEM signal can be completely described as

$$\boldsymbol{e}(t,r) = \left(E_\varphi \hat{\varphi} + E_\theta \hat{\theta}\right) s(t) \exp(\mathrm{j}(2\pi f t - \boldsymbol{k}^{\mathrm{T}} \boldsymbol{r}) \tag{5}$$

where E_φ and E_θ are respectively the polarization components in $\hat{\varphi}$ and $\hat{\theta}$ directions, $\boldsymbol{r}$ is the coordinate vector of any point in space, and $\boldsymbol{k}$ is the propagation vector. Jones polarization vector $\boldsymbol{h}$ can be expressed as

$$\boldsymbol{h} = \begin{bmatrix} E_\varphi \\ E_\theta \end{bmatrix} = \begin{bmatrix} \cos\gamma \\ \sin\gamma \mathrm{e}^{\mathrm{j}\eta} \end{bmatrix}. \tag{6}$$

Use the conversion matrix between spherical coordinate system and rectangular coordinate system $\boldsymbol{T}_z$, take the polarization vector of the orthogonal dipole emitting element in the XOZ plane as

$$\boldsymbol{s}_p = \begin{bmatrix} \sin\varphi & \sin\theta\cos\varphi \\ -\cos\varphi & \sin\theta\sin\varphi \end{bmatrix} \begin{bmatrix} \cos\gamma \\ \sin\gamma \mathrm{e}^{\mathrm{j}\eta} \end{bmatrix} = \boldsymbol{T}_z \cdot \boldsymbol{h}. \tag{7}$$

Then the combined steering vector of the polarization domain and airspace of the polarization array is

$$\boldsymbol{s}_{pa}(\gamma, \eta, \theta, \varphi) = \boldsymbol{s}_p \otimes \boldsymbol{a}(\Theta) \tag{8}$$

where $\boldsymbol{s}_{pa}(\gamma, \eta, \theta, \varphi) \in \mathbf{C}^{2MN \times 1}$ is the function of polarization parameters (γ, η) and the space parameter (θ, ϕ). $\otimes$ represents the Kronecker product.

The polarization domain-spatial domain joint matching weighting is performed on each electric dipole, and the weighting value is

$$\boldsymbol{w}_{pa} = \boldsymbol{s}_p(\gamma_0, \eta_0) \otimes \boldsymbol{a}(\theta_0, \varphi_0). \tag{9}$$

Therefore, the response function of the polarization array pattern of different polarizations and angles is

$$\boldsymbol{F}(\gamma, \eta, \theta, \varphi) = \left| \boldsymbol{w}_{pa}^{\mathrm{H}} \boldsymbol{s}_{pa}(\gamma, \eta, \theta, \varphi) \right|^2. \tag{10}$$

2.2 Adaptive polarization cancellation algorithm based on steepest gradient descent

For fixed polarization main lobe interference, if the interference is detected, the transmission of pulses will be stopped within a certain pulse period. The interference sampling data section is used to estimate the interference between the main array antenna and the auxiliary array antenna based on the minimum interference output power criterion. The cancellation weight coefficient $\boldsymbol{w}$ is applied to the echo data segment, and the horizontal polarization component of the auxiliary antenna is subjected to amplitude and phase processing to cancel the interference signal in the main channel. Its structure diagram is shown in Fig. 3.

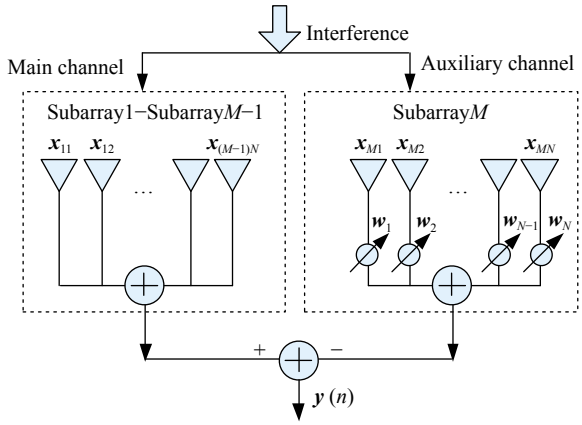

Fig. 3 Block diagram of adaptive polarization array cancellation structure

Generally, the interference of horizontally polarized echo is relatively large, so the main array antenna adopts vertical polarization, and the auxiliary array antenna adopts orthogonal polarization. The polarization states of each element of the main antenna and auxiliary antenna are represented by normalized Jones vectors as $\boldsymbol{h}_1$ and $\boldsymbol{h}_2$. The polarization state normalized Jones vector of the incident interference signal $J(n)$ is $\boldsymbol{h}_J$, and the average power is P_J. The interference signal received by each element of the main channel and the array output are

$$\boldsymbol{x}_{1i}(n) = \boldsymbol{h}_1{}^{\mathrm{T}}\boldsymbol{T}_{zj}\boldsymbol{h}_J\boldsymbol{a}_i(\Theta_J)J(n) + \boldsymbol{n}_{1i}(n), \tag{11}$$

$$\boldsymbol{X}_1(n) = \sum_{i=1}^{(M-1)N} \boldsymbol{x}_{1i}(n), \tag{12}$$

where $\boldsymbol{T}_{zj}$ is the coordinate system conversion matrix of the interference direction. The interference signals received by the N elements of the auxiliary channel are

$$\boldsymbol{x}_{Mi}(n) = \boldsymbol{h}_2{}^{\mathrm{T}}\boldsymbol{T}_{zj}\boldsymbol{h}_J\boldsymbol{a}_{(M-1)N+i}(\Theta_J)J(n) + \boldsymbol{n}_{2i}(n) \tag{13}$$

where $i = 1,2,\cdots,N$, $\boldsymbol{n}_{1i}(n)$ and $\boldsymbol{n}_{2i}(n)$ are the white noise of the main channel and auxiliary channel, and the average power is P_n . Then the output signal of the array polarization cancellation is

$$\boldsymbol{y}(n) = \frac{1}{N(M-1)}\boldsymbol{X}_1(n) - \sum_{i=1}^{N}\boldsymbol{w}_i(n)\boldsymbol{x}_{Mi}(n). \tag{14}$$

In (14), in order to make the iterative algorithm converge, the output signal of the main channel is averaged as the reference signal for cancellation. The APC iterative filtering model takes the interference output power as the minimum criterion, uses the steepest gradient descent, searches along the negative gradient direction of the cost function, and finally obtains the optimal solution of the cost function. The optimization problem can be expressed as

$$\min_{w} J(\boldsymbol{W}) = \mathrm{E}[|\boldsymbol{y}(n)|^2]. \tag{15}$$

The steepest gradient descent method is used to calculate (14) and (15), and the mathematical expectation is replaced by the instantaneous value to obtain the gradient estimate

$$\nabla_{w_i} J(\boldsymbol{W}) = \hat{\nabla}_{w_i}[\boldsymbol{y}^*(n)\boldsymbol{y}(n)] = -2\boldsymbol{y}(n)\boldsymbol{x}_{Mi}^*(n). \tag{16}$$

The weight vector update formula is

$$\boldsymbol{w}_i(n+1) = \boldsymbol{w}_i(n) - \mu\nabla_{w_i} J(\boldsymbol{W}) = \boldsymbol{w}_i(n) + 2\mu\boldsymbol{y}(n)\boldsymbol{x}_{Mi}^*(n) \tag{17}$$

where μ is the step factor, its value range [1] is set as $(0, 1/(P_J + P_n))$ to meet the convergence condition. When certain conditions are met, the iterative calculation is terminated, the weight vector is output, and the polarization cancellation is performed by substituting (18) to obtain the canceled output signal

$$\boldsymbol{y}'(n) = \frac{1}{N(M-1)}\boldsymbol{X}'_1(n) - \sum_{i=1}^{N}\boldsymbol{w}_i(n)\boldsymbol{x}'_{Mi}(n). \tag{18}$$

In (18), the expression of each signal is as follows:

$$\begin{aligned}\boldsymbol{x}'_{1i}(n) = {}& \boldsymbol{h}_1{}^{\mathrm{T}}\boldsymbol{S}\boldsymbol{T}_{zs}\boldsymbol{h}_1\boldsymbol{a}_i(\Theta_0)\boldsymbol{s}(n) + \\ & \boldsymbol{h}_1{}^{\mathrm{T}}\boldsymbol{T}_{zj}\boldsymbol{h}_J\boldsymbol{a}_i(\Theta_J)J(n) + \boldsymbol{n}_{1i}(n),\end{aligned} \tag{19}$$

$$\boldsymbol{X}'_1(n) = \sum_{i=1}^{(M-1)N}\boldsymbol{x}'_{1i}(n), \tag{20}$$

$$\begin{aligned}\boldsymbol{x}'_{Mi}(n) = {}& \boldsymbol{h}_2{}^{\mathrm{T}}\boldsymbol{S}\boldsymbol{T}_{zs}\boldsymbol{h}_1\boldsymbol{a}_{(M-1)N+i}(\Theta_0)\boldsymbol{s}(n) + \\ & \boldsymbol{h}_2{}^{\mathrm{T}}\boldsymbol{T}_{zj}\boldsymbol{h}_J\boldsymbol{a}_{(M-1)N+i}(\Theta_J)J(n) + \boldsymbol{n}_{2i}(n).\end{aligned} \tag{21}$$

In (19), $i = 1,2,\cdots,(M-1)N$, $\boldsymbol{S}$ is the polarization scattering matrix of the target, $\boldsymbol{T}_{zs}$ is the coordinate system conversion matrix of the target direction. $\boldsymbol{s}(n)$ is the radar modulation signal. In (21), $i = 1,2,\cdots,N$.

The output of the polarization cancellation process can be equivalently expressed as

$$\boldsymbol{y}' = \boldsymbol{T}_d\boldsymbol{X} \tag{22}$$

where $\boldsymbol{T}_d$ is the equivalent weight vector of the polarization cancellation process of the main and auxiliary channels. Its dimension is $1\times MN$. $\boldsymbol{X}$ is the received signal of all elements, its dimension is $MN\times L$, where L is the number of snapshots, so the expression can be written as

$$\boldsymbol{X} = [\boldsymbol{x}'_{11};\boldsymbol{x}'_{12};\cdots;\boldsymbol{x}'_{1(M-1)N};\boldsymbol{x}'_{M1};\boldsymbol{x}'_{M2};\cdots;\boldsymbol{x}'_{MN}]. \tag{23}$$

The equivalent weight vector can be calculated from (18) and (23), and its expression is shown in (24). Since $\boldsymbol{X}$ is not a square matrix, the pseudo-inverse of $\boldsymbol{X}$ is required here.

$$\boldsymbol{T}_d = \boldsymbol{y}' \boldsymbol{X}^{-1} \tag{24}$$

Use conventional adaptive beamforming algorithms, such as least mean square (LMS) algorithm, to process the output signal $\boldsymbol{y}'(n)$ after cancellation. Other interference signals from sidelobes can be further suppressed. Let the weight vector of spatial filtering be $\boldsymbol{w}_z$, Its dimension is $1\times MN$. Then the dynamic weight vector of the polarization domain-airspace joint processing $\boldsymbol{w}_d$ is

$$\boldsymbol{w}_d = \boldsymbol{w}_z \cdot \boldsymbol{T}_d. \tag{25}$$

3. Spatial adaptive beamforming model based on SVRGD

Although the APC method is used to perform polarization cancellation processing on the array received signal, the main lobe interference is better suppressed, and combined with the conventional adaptive beamforming such as the LMS method, it solves the main beam caused by the main lobe interference direction. Although the problem of beam distortion is solved, the peak of the main beam is still offset, and the sidelobe level is still high. In addition, the LMS beamforming algorithm is usually based on standard gradient descent, and each step of iteration needs to calculate the gradient of all sample points. The cost is higher when the number of samples is large. Therefore, it is necessary to optimize the spatial adaptive beamforming with the help of intelligent optimization algorithms such as machine learning to obtain excellent anti-mainlobe interference performance.

3.1 SGD algorithm

In the field of machine learning, the purpose of convex learning is to minimize the cost function. The SGD method does not require accurate gradient values to update the iteration direction, but takes a step size in a random direction. That is, it randomly selects a sample point from the data set each time or the sample block performs gradient update to ensure that the expected value of the direction is equal to the gradient direction in each iteration. In the spatial adaptive beamforming stage, given L snapshots, the optimization problem under the minimum mean square error criterion can be expressed as

$$\min_{\boldsymbol{w}_z} \frac{1}{L}\sum_{i=1}^{L} J_i(\boldsymbol{W}_z) = \min_{\boldsymbol{w}_z} \frac{1}{L}\sum_{i=1}^{L} \mathrm{E}\left[|\boldsymbol{e}(i)|^2\right] = \min_{\boldsymbol{w}_z} \frac{1}{L}\sum_{i=1}^{L} \mathrm{E}\left[\left|\boldsymbol{d}(i) - \boldsymbol{w}_z^{\mathrm{H}}(i)\boldsymbol{y}_z(i)\right|^2\right] \tag{26}$$

where adaptive weight vector $\boldsymbol{w}_z(n) \in \mathbf{C}^{MN\times 1}$, $\boldsymbol{d}(i)$ is the expected signal, $\boldsymbol{y}_z(i)$ is the weighted output of each array element after polarization filtering, $\boldsymbol{y}_z(i) \in \mathbf{C}^{MN\times L}$.

The SGD algorithm process of minimizing $J(\boldsymbol{W})$ is described as follows.

(i) Parameters: scalar $\mu_z > 0$, integer $T > 0$

(ii) Initialization: $\boldsymbol{w}_z(1) = \boldsymbol{0}$

(iii) For $t = 1, 2, \cdots, T$

Randomly choose from a distribution, such that

$$\mathrm{E}[\, \boldsymbol{v}_t | \boldsymbol{w}_z(t)] \in \partial J[\boldsymbol{w}_z(t)]$$

Update $\boldsymbol{W}(t+1) = \boldsymbol{W}(t) - \mu_z \boldsymbol{v}_t$

(iv) Output $\bar{\boldsymbol{W}} = \dfrac{1}{T}\sum_{t=1}^{T} \boldsymbol{W}(t)$.

3.2 SVRGD algorithm

Aiming at the problem of the low convergence rate of the SGD algorithm, the idea of the SVRGD algorithm is to use the global gradient information to modify the gradient used for each model update to improve the accuracy of the gradient calculation. There is an internal iteration within each iteration. Before internal iteration, calculate the average gradient $\nabla J_L[\boldsymbol{w}_z(k)]$ of all samples with the current value $\boldsymbol{w}_z(k)$. The initial value of the internal iteration is assigned to the current $\boldsymbol{w}_z(k)$, and the gradient formula after each correction in the internal iteration is

$$\tilde{\boldsymbol{g}}_j = \nabla f_{ij}(\bar{\boldsymbol{w}}_z^j) - [\nabla f_{ij}(\boldsymbol{w}_z^t) - \nabla J_L(\boldsymbol{w}_z^t)] \tag{27}$$

$$\bar{\boldsymbol{w}}_z^{j+1} = \bar{\boldsymbol{w}}_z^j + 2\mu_1 \tilde{\boldsymbol{g}}_j \tag{28}$$

where $\nabla J_L(\boldsymbol{w}_z^t)$ is the average gradient calculated using the weight vector $\boldsymbol{w}_z^t$ of the previous round; $\nabla f_{ij}(\boldsymbol{w}_z^t) - \nabla J_L(\boldsymbol{w}_z^t)$ is the offset of gradient estimation $\nabla f_{ij}(\boldsymbol{w}_z^t)$, $\tilde{\boldsymbol{g}}_j$ is the modified gradient, which is an unbiased estimate. Use $\tilde{\boldsymbol{g}}_j$ to update the weight vector $\bar{\boldsymbol{w}}_z^{j+1}$. The basic algorithm process is described as follows.

(i) Initialization $\boldsymbol{w}_z^t(1) = \boldsymbol{0}, \boldsymbol{w}_z^j(1) = \boldsymbol{0}$

(ii) For $t = 1, 2, \cdots, T$

(iii) Calculate the gradient of the data batch

$$\nabla J_L(\boldsymbol{w}_z^t) = \frac{1}{L}\sum_{k=1}^{L} \boldsymbol{e}^*(k)\boldsymbol{y}_z(k) \tag{29}$$

(iv) Initialization $\bar{\boldsymbol{w}}_z^j \leftarrow \boldsymbol{w}_z^t$

(v) For $j = 1, 2, \cdots, J$

(vi) Randomly select i, j from set $\{1, 2, \cdots, L\}$

(vii) $\tilde{\boldsymbol{g}}_j = \nabla f_{ij}(\bar{\boldsymbol{w}}_z^j) - [\nabla f_{ij}(\boldsymbol{w}_z^t) - \nabla J_L(\boldsymbol{w}_z^t)]$

(viii) $\bar{\boldsymbol{w}}_z^{j+1} = \bar{\boldsymbol{w}}_z^j + 2\mu_1 \tilde{\boldsymbol{g}}_j$

(ix) End for

(x) $$\boldsymbol{w}_z^{t+1} = \frac{1}{J}\sum_{j=1}^{J} \bar{\boldsymbol{w}}_z^j \tag{30}$$

(xi) End for

3.3 SVRGD-based adaptive beamforming algorithm flow

Weight output $\boldsymbol{y}_z(n)$ for each element after polarization filtering. Obtain the autocorrelation matrix and estimate it with

$$\hat{\boldsymbol{R}}_{\boldsymbol{y}_z\boldsymbol{y}_z} = \frac{1}{L}\left[\boldsymbol{y}_z(n)\boldsymbol{y}_z^{\mathrm{H}}(n)\right]. \tag{31}$$

Iteration step μ_1 must be satisfied for value range $0 < \mu_1 < \mathrm{tr}(\hat{\boldsymbol{R}}_{\boldsymbol{y}_z\boldsymbol{y}_z})$, in order to ensure the convergence of the adaptive beamforming algorithm based on gradient and stochastic gradient. Among them $\mathrm{tr}(\hat{\boldsymbol{R}}_{\boldsymbol{y}_z\boldsymbol{y}_z})$ represents the trace of the matrix. The specific process of the weight iterative algorithm based on SVRGD is as follows:

Step 1 Set the iteration times J and T of the inner and outer loops of the algorithm, and initialize the weight coefficients of the outer loop and inner loop $\boldsymbol{w}_z^t(1) = \boldsymbol{0}, \boldsymbol{w}_z^j(1) = \boldsymbol{0}$.

Step 2 Carry out the outer loop, and obtain the average gradient of the whole data by (29), $\boldsymbol{e}(k)$ is calculated by (26).

Step 3 Assign the weight coefficient $\boldsymbol{w}_z^t$ in the outer loop to the weight coefficient $\bar{\boldsymbol{w}}_z^j$ in the inner loop.

Step 4 Enter the inner loop, randomly select a snapshot number to calculate the random gradient $\nabla f_{ij}(\bar{\boldsymbol{w}}_z^j)$ and $\nabla f_{ij}(\boldsymbol{w}_z^t)$.

$$\nabla f_{ij}(\bar{\boldsymbol{w}}_z^j) = \boldsymbol{e}(ij)\boldsymbol{y}_z(ij) = [\boldsymbol{d}(ij) - \bar{\boldsymbol{w}}_z^{j\mathrm{H}}\boldsymbol{y}_z(ij)]^*\boldsymbol{y}_z(ij) \tag{32}$$

$$\nabla f_{ij}(\boldsymbol{w}_z^t) = \boldsymbol{e}^*(ij)\boldsymbol{y}_z(ij) = [\boldsymbol{d}(ij) - \boldsymbol{w}_z^{t\mathrm{H}}\boldsymbol{y}_z(ij)]^*\boldsymbol{y}_z(ij) \tag{33}$$

Step 5 Use (27) to find the corrected gradient as $\tilde{\boldsymbol{g}}_j$.

Step 6 Substitute the obtained gradient $\tilde{\boldsymbol{g}}_j$ into the inner loop iterative (28) to obtain the inner loop filter weight $\bar{\boldsymbol{w}}_z^{j+1}$ at the next moment.

Step 7 Repeat iterative Steps 4−6 until the inner loop iteration number J is reached, calculate the average weight coefficient using (30), and assign it to the outer loop.

Step 8 Repeat Steps 2−7, output the weight coefficient $\boldsymbol{w}_z$ of the last outer loop as the optimal weight coefficient of adaptive beamforming.

Step 9 Calculate the output $\boldsymbol{y}(n)$ of the array. The specific formula is as follows:

$$\boldsymbol{y}_o(n) = \boldsymbol{w}_z^{\mathrm{H}}\boldsymbol{y}_z(n). \tag{34}$$

3.4 Adaptive beamforming algorithm based on APC and SVRGD

APC and SVRGD combined architecture is used for adaptive beamforming. Firstly, the array signal is processed by the APC structure, and the main lobe interference in the signal is eliminated by using the polarization characteristics of the signal; then the SVRGD structure is used for adaptive beamforming of the signal after the main lobe interference is eliminated. The SVRGD algorithm has a higher accuracy, so the side lobe suppression effect is better. Therefore, the adaptive beamforming method based on APC and SVRGD can reduce the main lobe offset and suppress the side lobe.

4. Simulation

The static pattern simulation parameters are set as M=16,N=16,λ=0.1 m, and d_x=d_z=λ/2. Set the transmit beam direction $(\theta_0, \varphi_0) = (90°, 90°)$, the polarization angle is $(\gamma_0, \eta_0) = (30°, 60°)$. Let the reception also adopt the same polarization matching reception.

4.1 Characteristic analysis of *XZ* axial polarization plane pattern

Use (10) to add the weighted outputs of the H and V channels of all array elements to obtain the output of the array. Take the absolute value and normalize it to form a polarized array space designated beam pattern, as shown in Fig. 4. Fig. 5 shows the beam pattern of the conventional area array.

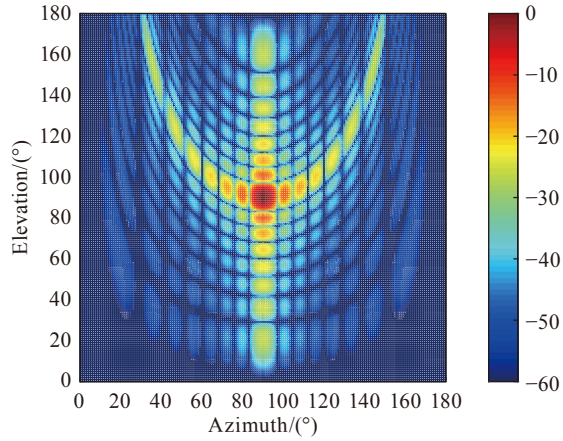

Fig. 4 16×16 HV three-dimensional pattern of channel polarization array

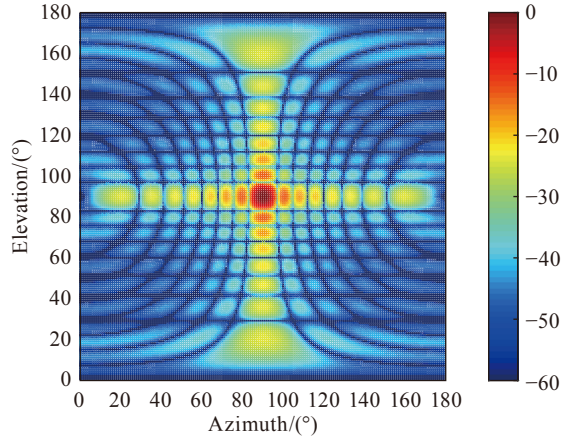

Fig. 5 16×16 three-dimensional pattern of conventional area array

It can be seen from the comparison of Fig. 4 and Fig. 5 that the main lobe width of the beam in the two modes are both $\theta_{3\mathrm{dB}} = \phi_{3\mathrm{dB}} = 6.42^\circ$. However, the side lobe distribution is significantly different. For polarized arrays, the antenna pattern gets the maximum value at the beam pointing (θ_0, φ_0) and main beam polarization parameters (γ_0, η_0). It has the capability of fully polarized transmitting and receiving, and has the capability of polarization diversity. In Fig. 5, the front surface is symmetrically distributed, and the static pattern of the azimuth angle and the elevation angle are completely consistent. The polarization mode of the electromagnetic wave cannot be controlled, but the beam direction can only be controlled.

4.2 Performance analysis of APC-SVRGD algorithm against main lobe interference

The APC-SVRGD algorithm and the APC-LMS algorithm, as well as the conventional area array SVRGD algorithm, are compared and analyzed in the beamforming and anti-mainlobe interference capabilities.

The receiving beamforming simulation settings are as follows: the target signal is a linear frequency modulation signal with a center frequency of 3 GHz and a bandwidth of 5 MHz; the interference source and noise are both Gaussian white noise, signal-to-noise ratio (SNR) SNR=0 dB, interference-to-noise ratio (INR) INR=10 dB; the snapshot number is L=1 024. The target pitch and azimuth are (90º, 90º). The target polarization scattering matrix $\boldsymbol{S} = \begin{bmatrix} 0.9 & -0.07\mathrm{j} & 0.04\mathrm{j} \\ 0.04\mathrm{j} & 0.9 & -0.06\mathrm{j} \end{bmatrix}$. Both interference sources are left-hand circularly polarized waves, $\boldsymbol{h}_{J1} = \boldsymbol{h}_{J2}\left[\sqrt{2}/2, (\sqrt{2}/2)\cdot \mathrm{e}^{\mathrm{j}\pi/2}\right]$. The pitch and azimuth of interference Source 1 are (90º, 88º), which is the main lobe interference. The pitch and azimuth values of interference Source 2 are (90º, 60º), which is the sidelobe interference. The purpose of setting the pitch angles of the target and the interference to be the same here is to facilitate the comparison with the beam level characteristics. The main channel antenna is vertically polarized where $\boldsymbol{h}_1$=[0,1]; the auxiliary channel antenna is horizontally polarized where $\boldsymbol{h}_2$=[1,0]. The number of inner loops J=L; the number of outer loops T=5 and the polarization cancellation iteration step $\mu_z = 10^{-9}$. The spatial adaptive beamforming iteration step $\mu_1 = 1/[4|\mathrm{tr}(\hat{\boldsymbol{R}}_{\boldsymbol{y}_z\boldsymbol{y}_z})|]$, which meets the convergence condition. The comparison of adaptive beamforming algorithms for 16×16 conventional area arrays is shown in Fig. 6, which is a characteristic diagram of the beam level at 90º elevation.

It can be seen from [18] that when the number of outer loops is small, the SVRGD algorithm has excellent beamforming ability, strong anti-sidelobe interference ability, and good robustness. When there is main lobe interference, it can be seen from Fig. 5 that although the SVRGD and LMS algorithms form deep nulls in both the main lobe and side lobe directions, the main beam shifts, and the offsets of the two are basically the same. The azimuth angle deviates from the true value by about 3.0º, and the sidelobe level is higher. The main beam offset of the SGD algorithm is smaller, but the null formation of sidelobe interference is slightly offset. The ability of the three algorithms to combat main lobe interference is poor.

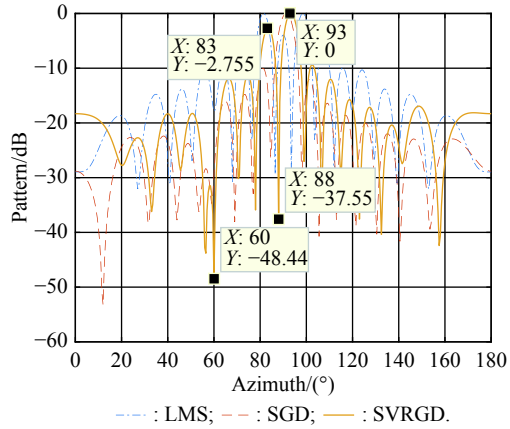

Fig. 6 Comparison of adaptive beamforming algorithms for conventional area arrays

Change the elevation and azimuth of the main lobe interference to (88º, 88º), and the elevation and azimuth of the side lobe interference to (60º, 60º), T=50; other conditions remain unchanged. The beamforming algorithms based on APC-LMS and APC-SVRGD are shown in Fig. 7 and Fig. 8.

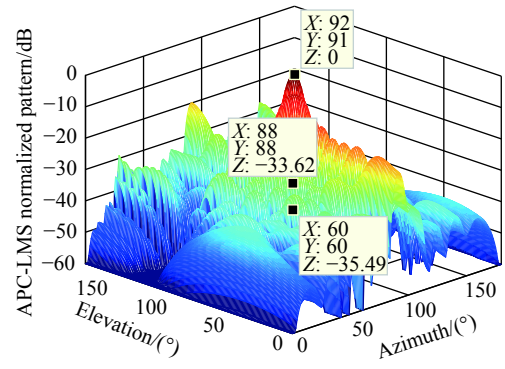

Fig. 7 APC-LMS algorithm adaptive beamforming

It can be seen from the comparison of Fig. 7 and Fig. 8 that the APC-LMS algorithm has no null formation in the interference direction of the main lobe, and the main

beam has no distortion, but the wave crest is slightly offset, the azimuth angle is offset by 1°, and the elevation angle is offset by 2°. However, the main beam of the APC-SVRGD algorithm does not shift and points accurately to the direction of the target wave. Both algorithms can adaptively zero the sidelobe interference, and the amplitude is less than 30 dB. Therefore, the APC-SVRGD algorithm is significantly better than the APC-LMS algorithm in terms of anti-main lobe interference performance improvement. The reason is that the average strategy is used to average the weight vectors randomly generated by all the inner loop snapshots in each outer loop. The initial value of an outer loop iteration, which avoids the phenomenon that oscillations, may occur near the global optimal value when the weight optimization iteration is closer to the global optimal value. After averaging, the optimal solution can be approached and the convergence speed can be improved.

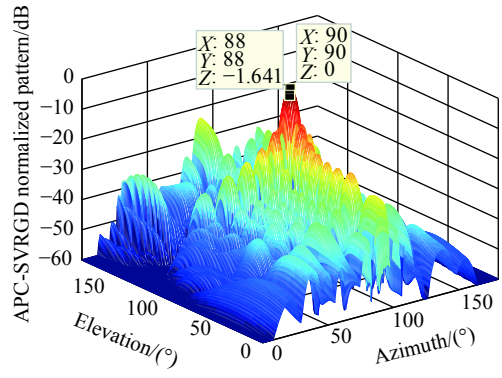

(a) Global figure

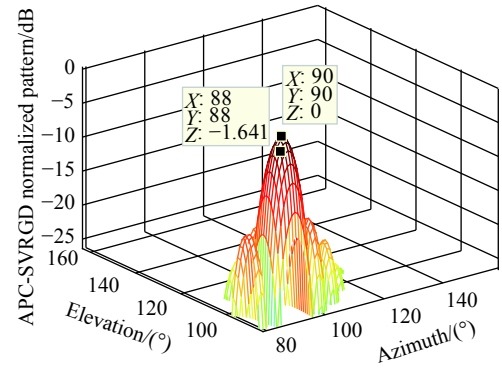

(b) Partial enlargement figure

Fig. 8 APC-SVRGD algorithm adaptive beamforming

4.3 Robustness analysis of APC-SVRGD algorithm

4.3.1 Analysis of the influence of the number of snapshots on the APC-SVRGD algorithm

When other conditions remain the same, set the number of snapshots to 2 000, 200, and 20 in sequence to obtain the target's horizontal characteristic beam pattern (when the pitch angle is 90°), as shown in Fig. 9.

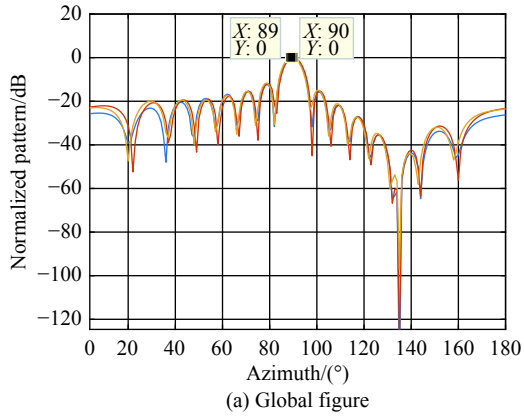

(a) Global figure

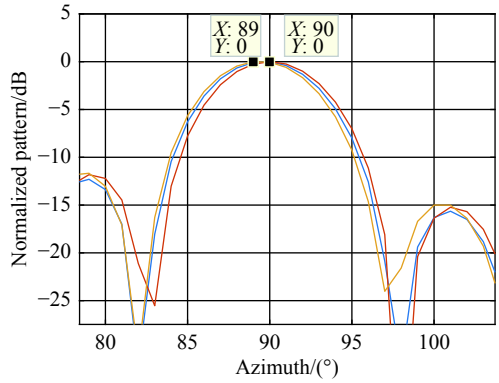

(b) Partial enlargement figure

—— : Snapshot number=20; —— : Snapshot number=200;
—— : Snapshot number=2 000.

Fig. 9 Horizontal pattern of beam formation at different snapshots

It can be seen from Fig. 9 that when the number of snapshots is 2 000 and 200, the azimuth angle forms the main beam at 90°, and the pointing is correct. When the number of snapshots decreases sharply to 20, the main beam shifts slightly, the peak shifts 1°, and the algorithm performance decreases slightly. It can be seen from the above that when the number of snapshots changes within a certain range, the SVRGD algorithm still has a good performance in the direction of the expected signal beam. This is mainly due to the existence of the outer loop and the sufficient number of iterations to maintain the beamforming effect.

4.3.2 Noise immunity analysis

When other conditions remain unchanged, set the SNR to −20 dB, 0 dB, and 25 dB respectively to obtain the target's horizontal characteristic beam pattern (when the elevation angle is 90°), as shown in Fig. 10. It can be seen that when the SNR is −20 dB , the main beam shifts. As the SNR decreases, the beamforming effect decreases.

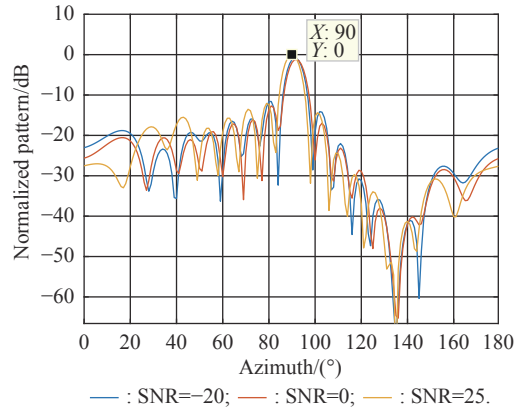

Fig. 10 Beamforming horizontal pattern under different SNRs

With other conditions remain unchanged, when the INR is set to 10 dB, 25 dB, and 40 dB, the horizontal characteristic beam pattern of the target (the elevation angle is 90°) is obtained, as shown in Fig. 11. It can be seen that the performance of the APC-SVRGD beamforming algorithm against mainlobe interference is easily affected by the INR. When the INR is low, the beam forming is accurate, but if the interference power is further increased, the main beam will shift, or even the beam cannot be formed.

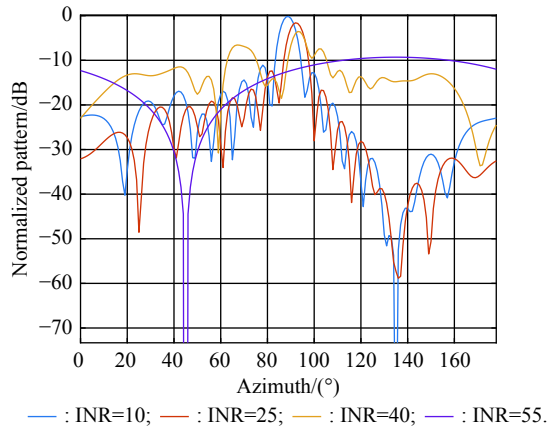

Fig. 11 Beamforming horizontal pattern under different INRs

5. Conclusions

Given the situation where airborne early warning radar is interfered by main/sidelobe in electronic warfare, a polarization array adaptive beamforming algorithm based on APC-SVRGD is proposed. Based on the polarization array structure of the main/auxiliary arrays, the weight vector of the auxiliary array is calculated through the APC iterative algorithm to eliminate the main lobe interference, and then the SVRGD method is introduced using the principle of SGD, and the gradient is corrected through the iteration of the inner and outer loops. In order to reduce the variance of the stochastic gradient estimation, and achieve the purpose of improving the gradient estimation approximation, through the combined processing of the polarization domain and the space domain, the adaptive nulling of the sidelobe interference is realized, and the main beam distortion, peak shift, and sidelobe level increase caused by the mainlobe interference are improved. The simulation results show that the method uses the inner and outer loop mechanism in the case of a small number of snapshots, so that the beamforming still has a good effect. It can achieve beamforming in the target direction under a certain signal to interference noise ratio, accurately. However, performance is easily affected by INR.

In addition, the signal processing structure of this method is mainly aimed at the situation of fixed polarization main lobe interference and single main lobe interference source. In practical applications, the radar may face multiple modes of supporting main lobe interference and variable polarization interference. How to improve the array structure optimization and intelligent optimization algorithms to combat strong main lobe interference and variable polarization interference still needs further research.

References

[1] TALISA S H, O'HAVER K W, COMBERIATE T M, et al. Benefits of digital phased array radars. Proceedings of the IEEE, 2016, 104(3): 530–543.

[2] ECKHARDT J M, NIKO J, ADRIAN F, et al. FMCW multiple-input multiple-output radar with iterative adaptive beamforming. IET Radar, Sonar & Navigation, 2018, 12(11): 1187–1195.

[3] HU B, WU X C, ZHANG X, et al. Adaptive beamforming based on compressed sensing with gain/phase uncertainties. IEICE Trans. on Fundamentals of Electronics, Communications and Computer Sciences, 2018, 101(8): 1257–1262.

[4] ASHWINI D, ZALAWADIA K. Performance analysis of LMS adaptive beamforming algorithm for smart antenna system. International Journal of Computer Applications, 2018, 179(28): 34–37.

[5] SHI W L, LI Y S, YIN J W. Improved constraint NLMS algorithm for sparse adaptive array beamforming control applications. Applied Computational Electromagnetics Society Journal, 2019, 34(3): 419–424.

[6] WANG Z G, ZHU C, DIAO Z L, et al. Summarization of anti-mainlobe-jamming technology of phased-array radar. Shipboard Electronic Countermeasure, 2019, 12(6): 13–18. (in Chinese)

[7] SHI L F, REN B, MA J Z. Recent developments of radar anti-interference techniques with polarimetry. Modern Radar, 2016, 38(4): 1–7. (in Chinese)

[8] ZONG Z W, SHI L F, WANG X S. A commonality used to discriminate active repetition false targets based on polarization characteristics of antenna. IET Radar, Sonar and Navigation, 2016, 10(7): 1178–1185.

[9] SHI L F, WANG X S, XU Z H, et al. A fast robust LMS adaptive beamforming algirithm. Journal of Electronics & Information Technology, 2006, 28(9): 1560–1564. (in Chinese)

[10] CHEN T Z. Adaptive dual-polarization canceller algorithm for counter mining radar jamming. Modern Defence Techno-

logy, 2018, 46(4): 67–72. (in Chinese)
[11] YANG Z, BAI W X, FU X L. Cancellation method analysis of full polarized auxiliary antenna to polarized interference. Modern Defence Technology, 2016, 44(5): 131–136. (in Chinese)
[12] REN B, SHI L F, WANG H G, et al. Investigation on polarization filtering scheme to suppress GSM interference in radar main beam. Journal of Electronics & Information Technology, 2014, 36(2): 459–464. (in Chinese)
[13] TANG Y Z, ZHAO G Z. Adaptive beamforming technique based on a modified particles warm optimization. Ship Science and Technology, 2018, 40(9): 111–115. (in Chinese)
[14] BAI M Y, LIU H, CHEN H C, et al. Adaptive beamforming algorithm based on deep neural network. Journal of Telemetry, Tracking and Command, 2019, 40(6): 28–35. (in Chinese)
[15] PHILIP C, JIM R, HUBERT D B. Estimating neural sources using a worst-case robust adaptive beamforming approach. Biomedical Signal Processing and Control, 2019, 52: 330–340.
[16] LIU S T, JIANG H L, LIU L B, et al. Gradient descent using stochastic circuits for efficient training of learning machines. IEEE Trans. on Computer-Aided Design of Integrated Circuits and Systems, 2018, 37(11): 2530–2541.
[17] MING Y W, ZHAO Y W, WU C K, et al. Distributed and asynchronous stochastic gradient descent with variance reduction. Neurocomputing, 2018, 281: 27–36.
[18] PENG F, WU J, WANG S, et al. Adaptive beamforming algorithm for airborne early warning radar based on SVRGD. Systems Engineering and Electronics, 2021, 43(1): 83–90. (in Chinese)
[19] SHI W L, LI Y S, SUN L J, et al. Norm constrained noise-free algorithm for sparse adaptive array beamforming. Applied Computational Electromagnetics Society Journal, 2019, 34(5): 709–715.
[20] YAO Z, SAXE A M, ADVANI M S, et al. Energy-entropy competition and the effectiveness of stochastic gradient descent in machine learning. Molecular Physics, 2018, 116(21): 3214–3223.
[21] BOTTARELLI L, LOOG M. Gaussian process variance reduction by location selection. Pattern Recognition Letters, 2019, 125(7): 727–734.
[22] CHEN X Z, SHU T, YU K B, et al. Enhanced ADBF architecture for monopulse angle estimation in multiple jammings. IEEE Antennas and Wireless Propagation Letters, 2017, 16: 2684–2687.
[23] KHAN Z A, CHAUDHARY N I, ZUBAIR S. Fractional stochastic gradient descent for recommender systems. Electronic Markets, 2019, 29(2): 275–285.
[24] YANG Z, WANG C, ZHANG Z M, et al. Random Barzilai-Borwein step size for mini-batch algorithms. Engineering Applications of Artificial Intelligence, 2018, 72(6): 124–135.
[25] MIN E X, LONG J, CUI J J. Analysis of the variance reduction in SVRG and a new acceleration method. IEEE Access, 2018, 4: 16165–16175.
[26] CHEN L, ZHOU S S, ZHANG Z. SVRG for a non-convex problem using graduated optimization algorithm. Journal of Intelligent & Fuzzy Systems, 2018, 34(1): 153–165.
[27] RAMAZANLI I, NGUYEN H, PHAM H, et al. Adaptive sampling distributed stochastic variance reduced gradient for heterogeneous distributed datasets. arXiv preprint arXiv: 2002.08528, 2020.
[28] YU K B. Mainlobe cancellation, orthgonal nulling and product patterns. Proc. of the IEEE International Symposium on Phased Array Systems and Technology, 2017. DOI: 10.1109/ARRAY.2016.7832637.
[29] YANG Z, WANG C, ZHANG Z M, et al. Accelerated stochastic gradient descent with step size selection rules. Signal Processing, 2019, 159(6): 171–186.
[30] LUO Z J, QIAN Y T. Stochastic sub-sampled Newton method with variance reduction. International Journal of Wavelets Multiresolution and Information Processing, 2019, 17(116): 62–68.

Biographies

PENG Fang was born in 1973. She received her M.S. and Ph.D. degrees in signal and information processing, communication, and information systems from Air Force Engineering University, Xi'an in 2005 and 2008, respectively. Since 2018, she has been an associate professor with the Aviation Engineering School, Air Force Engineering University. Her research interests include array signal processing and airborne early warning and detection technology.
E-mail: pengfang0916@163.com

WU Jun was born in 1972. He received his B.S. and M.S. degrees in radio communication, computer application from Air Force Engineering University, Xi'an in 1992 and 1996, respectively. Since 2018, he has been an professor of Air Traffic Control and Navigation School, Air Force Engineering University. His research interests include operational planning and mission planning.
E-mail: wuboy0210@163.com

WANG Shuai was born in 1996. He received his B.S. degree in communication engineering from Northeastern University in 2019. He is currently a postgraduate student in Air Force Engineering University. His research interest is array signal processing.
E-mail: 23202518172@qq.com

LI Zhijun was born in 1997. He received his B.S. degree in communication engineering from Air Force Engineering University in 2019. He is currently a postgraduate student in Air Force Engineering University. His research interest is array signal processing.
E-mail: 1812268525@qq.com

XIANG Jianjun was born in 1973. He received his M.S. and Ph.D. degrees in signal and information processing, communication, and information systems from Air Force Engineering University in 2001 and 2005, respectively. Since 2013, he has been an associate professor of Aviation Engineering School, Air Force Engineering University. His research interests focus on airborne early warning and detection technology.
E-mail: xiang787419@163.com